Limitations of the modulation method to smooth wire-guide roughness

I Bouchoule, J.-B Trebbia, Carlos L. Garrido Alzar

Limitations of the modulation method to smooth wire-guide roughness

I. Bouchoule, J.-B. Trebbia, and C. L. Garrido Alzar
Laboratoire Charles Fabry de l'Institut d'Optique, CNRS et Université Paris 11, 91127 Palaiseau Cedex, France
(Received 4 July 2007; published 27 February 2008)

It was recently demonstrated that wire-guide roughness can be suppressed by modulating the wire currents so that the atoms experience a time-averaged potential without roughness [Trebbia *et al.*, Phys. Rev. Lett. **98**, 263201 (2007)]. In this paper, we theoretically study the limitations of this technique. At low modulation frequency, we show that the longitudinal potential modulation produces heating of the cloud, and we compute the heating rate. We also give a quantum derivation of the rough conservative potential associated with the micromotion of the atoms. At large modulation frequency, we compute the loss rate due to nonadiabatic spin flip and show that it presents resonances at multiple modulation frequencies. These studies show that the modulation technique works for a wide range of experimental parameters. We also give conditions to realize radio-frequency evaporative cooling in such a modulated trap.

DOI: 10.1103/PhysRevA.77.023624 PACS number(s): 03.75.Be, 37.10.De

I. INTRODUCTION

Atom chips are a very promising tool for cooling and manipulating cold atoms [1]. Diverse potentials, varying on the micrometer scale, can be realized, and very high transverse confinements are possible. Applications envisioned range from integrated guided atomic interferometry [2–4] to the study of low-dimensional gases [5–7]. To benefit from the atom-chip technology, the atoms should be brought close to the current-carrying wires. But the atoms then experience a rough potential due to wire imperfections [8,9] and this used to constitute an important limitation of the atom-chip technology. However, a method to overcome this roughness problem, based on modulated currents, was recently demonstrated [10]. Due to the important envisioned applications of this method, a study of its limitations is crucial.

The method to suppress atomic wire-guide roughness consists in a fast modulation of the wire current around zero so that the atoms, as in a time-orbiting potential (TOP) trap [11], experience the time-averaged potential. Since the longitudinal potential roughness is proportional to the wire current [12], the time-averaged potential is exempt from roughness. The modulation frequency ω must be large enough so that the atomic motion cannot follow the instantaneous potential. On the other hand, ω should be small enough to prevent losses due to spin-flip transitions [13]. In this paper, we present an analysis that goes beyond the time-averaged potential approach, and we identify the limitations of this method, for both small and large ω. We also investigate the possibility of using the radio-frequency evaporative cooling method in such a modulated trap.

In Sec. II, we present the considered situation. In Sec. III, we investigate the limitations of the method that arise at small modulation frequency. Using a Floquet analysis, we show that the atomic cloud is submitted to a heating that we study quantitatively. Within this formalism, we also recover the well-known adiabatic potential experienced by atoms in rapidly modulated fields. In our case, it amounts to a residual roughness. In Sec. IV, we compute the expected spin-flip losses due to the time modulation of the magnetic field orientation that arise at large ω. Finally, the last section gives some insights into the possibility of realizing radio-frequency evaporative cooling in the modulated guide.

II. WIRE GUIDE

A wire guide can be obtained by combining a transverse quadrupolar field and a homogeneous longitudinal magnetic field B_0. The quadrupolar field can be realized using, for example, three current-carrying wires as shown in Fig. 1. Because of wire deformations [9,14], the current density inside the wires acquires nonzero transverse components. This produces a longitudinal rough magnetic field b_z proportional to the wire current, much smaller than the external field B_0. The method to effectively remove the roughness consists in modulating the currents at a frequency ω while the longitudinal field B_0 is kept constant.

III. EFFECT OF THE MODULATION ON THE LONGITUDINAL MOTION

Let us first assume that the modulation frequency of the wire currents is small enough so that the atomic spin orientation can follow the magnetic field orientation adiabatically. The atoms are then subjected to the instantaneous potential $\mu|\mathbf{B}|$, where μ is the atomic magnetic dipole moment. For B_0 much larger than E/μ, where E is the typical transverse atomic energy, the instantaneous transverse potential is harmonic and proportional to the instantaneous wire currents.

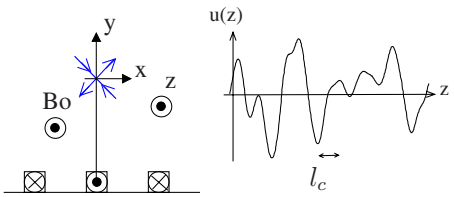

FIG. 1. (Color online) A wire guide produced by three current-carrying wires. Geometrical deformation of the wire produces a longitudinal potential roughness (of correlation length l_c) proportional to the wire current as depicted in the figure.

Since the oscillation frequency of this potential is modulated in time, the transverse classical dynamics is described by a Mathieu equation, which predicts stable motion as long as $\omega > 0.87\omega_\perp$, where $\omega_\perp$ is the maximum instantaneous transverse oscillation frequency. This classical criterion is also predicted by quantum mechanics since the Wigner function evolves as a classical phase space distribution for a harmonic potential [15]. In this paper, we assume this stability condition is satisfied. We also assume that the longitudinal dynamics is decoupled from the transverse one and we focus on the longitudinal motion. The longitudinal instantaneous potential

$$V(z,t) = u(z)\cos(\omega t), \tag{1}$$

where $u(z)=\mu b_z(z)$, sketched in Fig. 1, is produced by wire deformations. The idea of the method to smooth the roughness is that the longitudinal motion of the atoms does not have time to follow the time evolution of the potential. The atomic motion is then well described by the effect of the conservative potential $\langle V(z,t)\rangle$, where the time average is done over a modulation period. Since $\langle V(z,t)\rangle=0$, the atoms do not experience any roughness. We study below the conditions on the modulation frequency ω for such an approach to be valid.

As the Hamiltonian experienced by the atoms is periodic in time, we use the well-known Floquet representation [16], briefly presented below for the situation considered here. A new quantum number n_F is introduced, which gives the relative number of modulation energy quanta. The Hamiltonian in this representation is time independent and contains two contributions. The first one,

$$H_0 = \sum_{n_F=-\infty}^{\infty} [p^2/(2m) + \hbar\omega n_F]|n_F\rangle\langle n_F|, \tag{2}$$

does not couple different Floquet subspaces. The second one,

$$H_1 = \sum_{n_F=-\infty}^{\infty} u(z)/2(|n_F\rangle\langle n_F+1| + |n_F+1\rangle\langle n_F|), \tag{3}$$

couples adjacent Floquet subspaces. If the state of the system in the Floquet representation is $\Sigma_{n_F}|\psi_{n_F}\rangle(t)|n_F\rangle$, where $|\psi_{n_F}\rangle(t)$ gives the state of the system in the manifold of Floquet number n_F, then the state of the system in the bare representation is $\Sigma_{n_F}|\psi_{n_F}\rangle(t)e^{-in_F\omega t}$. Expectation values of observables contain cross terms involving different Floquet numbers. However, as long as evolution on time scales much larger than $1/\omega$ is considered, such cross terms (interference terms) average to zero, and the different Floquet states can be interpreted as physically different states. A given state has an infinite number of Floquet expansions. In particular, it is possible to assume that the initial state is in the Floquet manifold of Floquet number $n_F=0$.

Let us consider a state $|p_0,n_F=0\rangle$ of momentum p_0 in the Floquet manifold $n_F=0$. The modulated rough potential u is responsible for two different phenomena. First, it induces an exchange energy rate of the atomic energy. This irreversible evolution is due to the continuous nature of the rough-potential Fourier decomposition: the state $|p_0,n_F=0\rangle$ is coupled to a continuum of momentum states of the adjacent Floquet subspaces $n_F=\pm 1$ and this coupling to a continuum induces a departure rate from the initial state associated with the rate of kinetic energy change. Second, the modulated potential is responsible for the well-known adiabatic potential experienced by atoms in rapidly modulated fields [17]. We show that this adiabatic potential is due to processes of order 2 in u that couple the state $|p_0,n_F=0\rangle$ to the states $|p_1,n_F=0\rangle$ via the virtually populated intermediate states $|q,n_F=\pm 1\rangle$.

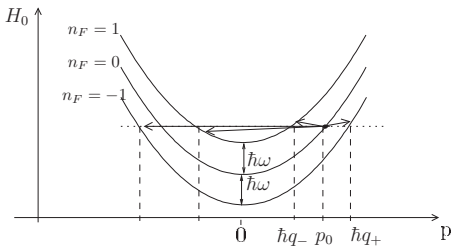

FIG. 2. Transitions responsible for a heating of the atomic cloud. The parabolas give the energy H_0, given in Eq. (2), versus the momentum p for different Floquet manifolds n_F. The state of momentum p_0 in the Floquet manifold $n_F=0$ is coupled to different momentum states of the Floquet manifolds $n_F=\pm 1$ by the rough potential $u(z)$.

In the first section, we investigate the first phenomenon and compute the associated heating rate for a cloud at thermal quasiequilibrium. In the second section, we derive the adiabatic potential experienced by the atoms. In both sections, we emphasize the case where the potential roughness is that obtained at large distances from a flat wire having white noise border fluctuations.

A. Heating of the atomic cloud

Let us suppose the atom is initially in the state $|p_0,n_F\rangle$ of momentum p_0 in the Floquet manifold $n_F=0$. As shown in Fig. 2, this state is coupled by u to the continuum of momentum states in the Floquet manifold $n_F=\pm 1$, which leads to a decay of the initial state population. The momenta of the final states that satisfy energy conservation in the Floquet subspace $n_F=-1$ are $\pm\hbar q_+$, where $q_+=\sqrt{k_0^2+2m\omega/\hbar}$, $k_0=p_0/\hbar$ being the initial atomic wave vector. Decay toward these states involves the Fourier component $\pm q_+ - k_0$ of u and increases the kinetic energy of the atom by $\hbar\omega$. If $k_0^2 > 2m\omega/\hbar$, there exist states in the Floquet subspace $n_F=1$ that have the same energy as the initial state. The momenta of those final states are $\pm\hbar q_-$ where $q_-=\sqrt{k_0^2-2m\omega/\hbar}$, and decay toward these states decreases the kinetic energy of the atom by $\hbar\omega$. A perturbative calculation, identical to the one used to derive Fermi golden rule, gives an energy exchange rate

$$\frac{dE}{dt} = \frac{\pi\omega m}{2\hbar^2}\{[S(-k_0+q_+)+S(-k_0-q_+)]/q_+ - \Theta(|k_0|-\sqrt{2m\omega/\hbar})[S(-k_0+q_-)+S(-k_0-q_-)]/q_-\}, \tag{4}$$

where $S(q)=(1/2\pi)\int e^{iqz}\langle u(0)u(z)\rangle dz$ is the spectral density

of u, characterized by the correlation length l_c, and $\Theta(x)$ is the Heaviside function, which is zero for $x<0$ and 1 for $x>0$. The derivation of Eq. (4) is detailed in Appendix A. As pointed out in the appendix, Eq. (4) is not valid for an initial momentum very close to $\sqrt{2m\hbar\omega}$. However, the range of k_0 for which the formula is not valid is in general very small and we ignore this in the following.

Apart from the rms amplitude of the roughness, which accounts only for a multiplicative factor in the rate of the energy change, three energies are relevant: $E_\omega=\hbar\omega$ is the energy quantum corresponding to the modulation frequency, $E_m=ml_c^2\omega^2$ is about the kinetic energy of an atom that would travel over l_c during an oscillation period, and $E_c=p_0^2/(2m)$ is the atomic kinetic energy. In the following, we consider two different limits for which we give simplified expressions for the energy change rate: the classical limit and the quantum low-energy limit.

Let us first assume that $E_\omega/\sqrt{E_mE_c}\ll 1$ and $E_\omega E_m^{1/2}/E_c^{3/2}\ll 1$. We show below that these two conditions ensure the validity of the classical behavior. These two conditions ensure that $E_\omega/E_c\ll 1$ so that q_+ and q_- are close to k_0 and one can expand the quantity $q_\pm/k_0$ in powers of $m\omega/(\hbar k_0^2)$. Since the wave vectors $-k_0-q\pm$ and $-k_0+q\pm$ are separated by about $2k_0$, the first condition ensures that the spectral components $S(-k_0-q\pm)$ are negligible compared to the two others. The second condition ensures that the latter are well approximated using a Taylor expansion of S. Finally, the energy exchange rate is written as

$$\frac{dE}{dt}=-[2\omega^2/v_0^3S(\omega/v_0)+S'(\omega/v_0)\omega^3/v_0^4]\pi/(2m), \quad (5)$$

where $v_0=\hbar k_0/m$ is the atomic velocity. This energy exchange rate does not depend on $\hbar$ and is thus a classical result. It is obtained through a classical calculation of kinetic energy exchange computed after expanding the atomic trajectory to second order in u. Note that, using the classical expression $E_c=mv_0^2/2$, the two conditions $E_\omega/\sqrt{E_cE_m}\ll 1$ and $E_\omega E_m^{1/2}/E_c^{3/2}\ll 1$ are verified in the limit where $\hbar$ goes to zero, as expected for the validity of classical physics.

Let us now consider the limit $E_\omega/E_c\gg 1$ and $E_cE_m^{1/2}/E_\omega^{3/2}\ll 1$, which we denote the quantum low-energy limit. The first inequality ensures that the Heaviside function in Eq. (4) is zero and that q_+ can be replaced by $\sqrt{2\hbar\omega}$ in the denominator. The second inequality ensures that this replacement is also valid for the argument of the S function. Then the energy exchange rate given by Eq. (4) reduces to

$$\frac{dE}{dt}=\frac{\pi\sqrt{m\omega}}{\sqrt{2\hbar^3}}[S(-k_0+\sqrt{2m\omega/\hbar})+S(k_0+\sqrt{2m\omega/\hbar})]. \quad (6)$$

This is a quantum result, sensitive to the fact that energy exchange between the atom and the oscillating potential involves the energy quanta $\hbar\omega$. In the limit where $E_c\ll E_\omega^2/E_m$ $(k_0\ll 1/l_c)$, it converges toward a finite value

$$\frac{dE}{dt}=\frac{\pi\sqrt{2m\omega}}{\sqrt{\hbar^3}}S(\sqrt{2m\omega/\hbar}) \quad (7)$$

that does not depends on the initial momentum $\hbar k_0/m$.

Let us now consider a cloud initially at thermal equilibrium with a velocity distribution $n(v_0)$. The heating rate, obtained after averaging Eq. (4) over $n(v_0)$, is

$$k_B\frac{dT}{dt}=2\int_0^\infty n(v_0)\frac{dE}{dt}dv_0, \quad (8)$$

where k_B is the Boltzmann factor. Although the heating rate depends on the precise shape of the spectral density S, some general properties can be derived.

First, although the energy exchange rate may be negative for some velocities, we show below that dT/dt is always positive. For a longitudinally homogeneous gas, this positivity ensures the increase of the entropy, as required by the second law of thermodynamics in the absence of heat exchange with the cloud and without gaining information on the system. To demonstrate that $dT/dt>0$, we perform a change of variables in the four integrals obtained by substituting Eq. (4) into Eq. (8) to find

$$\begin{aligned}k_B\frac{dT}{dt}=(\pi\omega m/\hbar)\Bigg(&\int_0^{Q_0}\frac{dq}{q}S(q)[n(\omega/q-\hbar q/2m)\\&-n(\omega/q+\hbar q/2m)]\\&+\int_{Q_0}^\infty\frac{dq}{q}S(q)[n(\hbar q/2m-\omega/q)\\&-n(\omega/q+\hbar q/2m)]\Bigg),\end{aligned} \quad (9)$$

where $Q_0=\sqrt{2m\omega/\hbar}$. For a thermal equilibrium distribution, $n(v)$ is a decreasing function of $|v|$. Furthermore, the spectral density is a positive function. We thus find that $dT/dt>0$ so that the effect of the potential roughness is always a heating of the cloud. Equation (9) also shows that the heating rate goes to zero at very large temperatures, since n is then about flat over the explored velocities.

Second, for large enough temperatures one expects to recover the classical result and the heating rate should not depend on $\hbar$. Then the heating rate depends only on the four independent quantities $\langle u^2\rangle$, E_m, ω, and k_BT. Since $\langle u^2\rangle$ enters only as a multiplicative factor in the heating rate, using dimensional analysis we show that k_BdT/dt is the product of $\langle u^2\rangle/(m\omega l_c^2)$ and a function of k_BT/E_m. As a consequence, if the function giving the heating rate versus T is known for a given value of ω and E_m, then the heating rate is known for any value of T, E_m, and ω.

Finally, at low enough temperatures, the heating rate is well estimated by substituting Eq. (6) into Eq. (8). One expects that the heating rate converges toward Eq. (7) when the temperature becomes much smaller than $\hbar\omega$ and $\hbar^2/(ml_c^2)$.

In the following, we give quantitative results in the case of a potential roughness obtained at large distances d from a flat wire whose borders have white noise fluctuations of spectral density J_f. In this condition, the spectral density of u is given by [8,9]

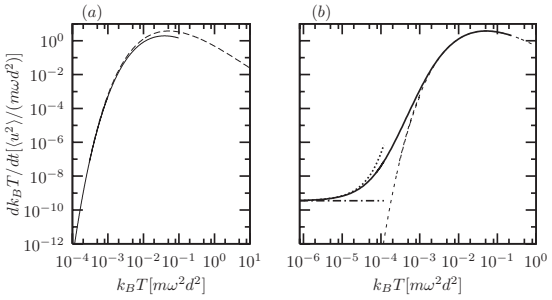

FIG. 3. Heating rate of a cloud as a function of its temperature, for a modulated rough potential whose spectral density is given by Eq. (11). (a) Classical predictions (dashed lines) and asymptotic behavior at low temperature given by Eq. (12) (solid line). (b) Exact result for $\omega/(2\pi)=200\hbar/(md^2)$ (solid line) compared with the quantum low-energy prediction (dotted line), the asymptotic prediction of Eq. (13) (dash-dotted line), and the classical result (dashed line).

$$S(k) = J_f \frac{(\mu_0 \mu I)^2}{4\pi^2} k^4 K_1(kd)^2, \tag{10}$$

where K_1 is the modified Bessel function of the first kind. The typical correlation length of u is the distance above the wire d so that $E_m=m\omega^2d^2$. The mean square of the rough potential is $\langle u^2\rangle \simeq 0.044(\mu\mu_0 I)^2 J_f/d^5$. In the following we use $\langle u^2\rangle$ as a parameter instead of J_f. The spectral density of u is then

$$S(k) = \alpha \langle u^2\rangle d(kd)^4 K_1(kd)^2, \tag{11}$$

where $\alpha \simeq 23$.

We first study the heating rate predicted by classical physics. This classical heating rate is plotted in Fig. 3(a) as a dashed line. The temperature and heating rate are scaled to E_m and $\omega\langle u^2\rangle/E_m$, respectively, so that the curves corresponding to the classical predictions are independent of the problem parameters. We observe the expected decrease to zero of the heating rate at high temperatures. We also observe a rapid decrease of the heating rate as the temperature decreases, for temperatures much smaller than E_m. The maximum heating rate is about $2.1\langle u^2\rangle/(m\omega d^2)$ and is obtained for the temperature $k_BT_M \simeq 0.07E_m$. For $d=5$ μm and $\omega/(2\pi)=50$ kHz, which are parameters similar to those of the experiment presented in [10], $T_M=1.8$ mK. Typical cold atom temperatures are much smaller than this value, and it is thus of experimental interest to investigate in more detail the regime $T \ll T_M$.

The decrease of the heating rate for $T \ll T_M$ is expected since, in this case, the atoms move over a distance much smaller than the correlation length of the rough potential during a modulation period. The atoms are then locally subjected to an oscillating force almost independent of z, and the atomic motion can be decomposed into a fast micromotion in counterphase with the modulation and a slow motion. Since the micromotion is almost in counterphase with the excitation force, almost no energy exchange between the atom and the potential arises on a time scale larger than the modulation period. More quantitatively, we can derive an analytical expression for the heating rate in the regime where $T \ll T_M$, which shows the decrease of the heating rate as temperature decreases. For such low temperatures, as shown *a posteriori* below, wave vectors in S that contribute to the heating rate are much larger than $1/d$ so that we can replace the Bessel function $K_1(x)$ in Eq. (11) by its asymptotic value at large x. We then find that the integrand in Eq. (8) is peaked around $v_0=2^{1/3}(k_BT\sqrt{E_m})^{1/3}/m$ and the Laplace method gives the following approximation for the heating rate:

$$\frac{k_B dT}{dt} = \beta \frac{\omega\langle u^2\rangle}{E_m} \left(\frac{E_m}{k_BT}\right)^{7/3} e^{-3(E_m/2k_BT)^{1/3}}, \tag{12}$$

where $\beta \simeq 0.36$. This asymptotic function is plotted in Fig. 3(a) (solid line). It coincides with the exact classical result within 20% as long as $k_BT < 0.002E_M$. The above expression of v_0 and Eq. (5) validate the expansion at large x of the Bessel function $K_1(x)$ for $T \ll T_M$.

The limit of validity of the classical results described above is given by $E_\omega/\sqrt{E_cE_m} \ll 1$ and $E_\omega E_m^{1/2}/E_c^{3/2} \ll 1$, where $E_c \simeq mv_0^2$, v_0 being the typical velocity involved in the heating process. Using the above value for v_0, the condition of validity of the classical regime is reduced, for $E_\omega \ll E_m$, to $k_BT \gg E_\omega$. For $\omega/2\pi=50$ kHz, we find that the classical regime fails for temperatures $T \ll 2$ μK. At lower temperatures, quantum analysis is required to estimate the heating rate.

For the above parameters ($d=5$ μm and $\omega/2\pi=50$ kHz), $E_m/E_\omega=10^4$ and the heating rate is exponentially small at temperatures smaller than 1 μK, where classical physics fails [the term $e^{-3(E_m/2k_BT)^{1/3}}$ in Eq. (12) is 3×10^{-31} for $T=1$ μK]. Thus, in order to investigate the heating rate beyond the classical approximation, we consider a different situation for which E_m/E_ω is only equal to 200. This would correspond, for the same distance $d=5$ μm, to a modulation frequency of only 1 kHz. The exact heating rate, which is computed by substituting Eq. (4) into Eq. (8), is plotted in Fig. 3(b). This calculation shows that the classical result is valid up to a factor of 2 as long as $k_BT > 0.2E_\omega$. At lower temperatures, the classical result underestimates the heating rate. At temperatures much smaller than $E_\omega^{3/2}/\sqrt{E_m}$, the heating rate is well approximated by the predictions in the low-energy quantum limit where Eq. (6) is valid. This prediction is represented as a dotted line in the graph. At temperatures much smaller than E_ω^2/E_m (i.e., for $k_BT \ll \hbar^2/md^2$), the heating rate converges toward Eq. (7). Assuming $E_m/E_\omega \gg 1$, then the expansion of S at large wave vector can be used and Eq. (7) gives

$$k_B dT/dt = \zeta\langle u^2\rangle/\hbar(m\omega d^2/\hbar)^2 e^{-2\sqrt{m\omega d^2/\hbar}} \tag{13}$$

where $\zeta \simeq 4.0$. This asymptotic value is plotted in Fig. 3 as dash-dotted lines. The heating rate is equal to this limit up to a factor of 2 as soon as $k_BT < 0.2E_\omega^2/E_m$.

The heating of the atomic cloud can easily be made small enough experimentally to have no noticeable effects. Let us for example consider the situation, similar to the experiment in [10], where $d=5$ μm and $\sqrt{\langle u^2\rangle}=50$ nK. If the modulation frequency is as low as 1 kHz, then the maximum heating rate is 3 μK/s and is obtained for a temperature of 700 nK.

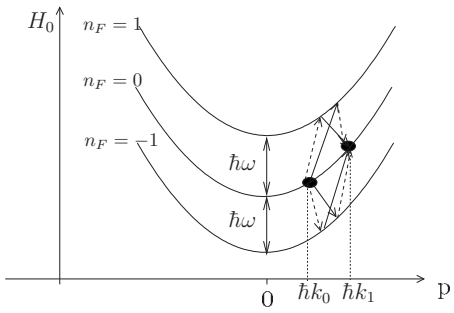

FIG. 4. Raman transitions responsible for the adiabatic potential of Eq. (14). The second-order coupling between two momentum states of wave vector k_0 and k_1 is sketched. The coupling produced by two Fourier components of u of wave vector q and $q'=k_1-q-k_0$ are represented as dashed and solid arrows, respectively.

Thus, for such a low modulation frequency, the heating may be a problem in experiments using the modulation technique. However, as soon as the modulation frequency is increased to 50 kHz, as in [10], the maximum heating rate is only 64 nK/s and is obtained at a large temperature of 1.8 mK. At lower temperatures, the exponential decrease of the heating rate shown in Eq. (12) rapidly decreases the heating rate to completely negligible values.

B. Effective remaining potential

In this section, we show that Raman processes (of second order in u), in which adjacent Floquet states are virtually populated, are responsible for an effective potential

$$V_{\mathrm{ad}}=(\partial u/\partial z)^2/4m\omega^2. \tag{14}$$

This potential is a well-known classical result [17] that corresponds to the kinetic energy of the micromotion of a trapped particle. The micromotion has been seen, for example, in Paul traps [18,19] and in TOP traps [20,21]. In our situation, at large oscillation frequency, the micromotion has an amplitude $\xi\simeq-(\partial u/\partial z)/(m\omega^2)\cos(\omega t)$ much smaller than the correlation length of u. It is in counterphase with the excitation force and has a kinetic energy V_{ad}. In this limit, since the micromotion is in counterphase with the excitation force, the energy transfer between the atom and the potential, averaged over a modulation period, vanishes. Energy conservation then shows that the slow motion of the atom is subjected to an effective rough potential V_{ad}. It is well known that this effective potential, due to the fast atomic micromotion, is responsible for the confinement in rapidly modulated Paul traps. A quantum derivation of V_{ad} has already been done in [15] using a secular approximation. Here we give an alternative derivation based on the Floquet representation.

Let us compute the effective coupling between the states $|k_0\rangle$ and $|k_1\rangle$ of momenta $\hbar k_0$ and $\hbar k_1$, respectively, both being in the Floquet subspace $n_F=0$. For this purpose, we first investigate the effect of a given pair of Fourier components of u that couple the two previous states. Their wave vectors are q and $q'=k_1-k_0-q$. Four processes are involved in the effective coupling between $|k_0\rangle$ and $|k_1\rangle$, as sketched in Fig. 4, and the effective coupling is the sum of the four amplitudes. The precise effective coupling between two "ground" states coupled via an intermediate level has been investigated in [22]. The authors show that the effective coupling is V_1V_2/Δ, where V_1 and V_2 are the coupling to the intermediate state and Δ is the difference between the energy of the intermediate state and the mean energy of the two ground states. Using this result, we find that the effective coupling associated with each process is

$$v_{\mathrm{eff}}=u_qu_{q'}/\{4[\hbar^2(k_0+\kappa)^2]/(2m)\pm\hbar\omega-E_0\}, \tag{15}$$

where κ is q or q' depending on the process and $E_0=\hbar^2(k_0^2+k_1^2)/4m$. Adding the four amplitudes, we find

$$V_{\mathrm{eff}}=\frac{u_qu_{q'}}{4}\left(\frac{\hbar^2(k_0+q)^2/m-2E_0}{[\hbar^2(k_0+q)^2/(2m)-E_0]^2-\hbar^2\omega^2}+\frac{\hbar^2(k_0+q')^2/m-2E_0}{[\hbar^2(k_0+q')^2/(2m)-E_0]^2-\hbar^2\omega^2}\right). \tag{16}$$

Assuming that the kinetic energies of the final, initial, and intermediate states are all much smaller than $\hbar\omega$, the denominator can be simplified to $-\hbar^2\omega^2$, and we obtain

$$V_{\mathrm{eff}}=\frac{u_qu_{q'}qq'}{2m\omega^2}. \tag{17}$$

Doing the sum over the pairs (q,q'), we find that the coupling between the momentum states is that realized by the potential of Eq. (14).

An alternative way to derive the adiabatic potential is to use a dressed Floquet representation. As shown in Appendix B, the calculations are more straightforward in this representation. In addition, no detailed knowledge of the effective coupling corresponding to a transition through a virtually populated state is required.

The residual roughness given in Eq. (14) constitutes a limitation of the modulation method. It scales as $\langle u^2\rangle/(ml_c^2\omega^2)$, where l_c is the typical correlation length of u. Thus it is much smaller than the initial roughness amplitude as soon as $\sqrt{\langle u^2\rangle}\ll ml_c^2\omega^2$. In the case where the roughness potential spectral density is that obtained at large distances from a wire having white noise border fluctuations of spectral density J_f, we obtain a mean value

$$\langle V_{\mathrm{eff}}\rangle=0.048J_f\frac{(\mu_0\mu I)^2}{m\omega^2d^7}=1.1\langle u^2\rangle/(m\omega^2d^2). \tag{18}$$

If the wire edge deformations have a Gaussian probability distribution, then the roughness of the remaining potential is simply $\sqrt{\langle V_{\mathrm{eff}}^2\rangle-\langle V_{\mathrm{eff}}\rangle^2}=\sqrt{2}\langle V_{\mathrm{eff}}\rangle$. For $d=5$ μm, $\omega/(2\pi)=50$ kHz, and $\sqrt{\langle u^2\rangle}/k_B=500$ nK, the roughness of the effective remaining potential is as small as 0.09 nK.

IV. LOSSES DUE TO SPIN-FLIP TRANSITIONS

All the previous analysis assumes that the atomic spin can adiabatically follow the direction of the instantaneous field when the current is modulated. In this section, we investigate the conditions on the modulation frequency for this adiabatic following requirement to be valid. Nonadiabaticity induces

losses via spin-flip transitions to the untrapped states. Intuitively, we expect that the losses are small for a modulation frequency much smaller than the Larmor frequency. In the following, we compute this loss rate, following calculations done in [23] for the dc case.

Let us consider a spin-1 atom in the modulated guide described in Sec. II with $\omega \gg \omega_\perp$. We choose a coordinate system whose origin is at the quadrupole field center and with axes x and y at 45° to the quadrupole axis as depicted in Fig. 1. We assume the atomic magnetic moment is $\mu \mathbf{J}/\hbar$ where $\mathbf{J}$ is the atomic spin angular momentum of components J_x, J_y, and J_z along x, y, and z, respectively. We denote by $|\pm 1\rangle$ and $|0\rangle$ the eigenstates of J_z of eigenvalues $\pm\hbar$ and 0, respectively.

The magnetic field direction depends on position and on time. We apply a space- and time-dependent spin rotation $\mathcal{R}(t,x,y)$ so that $\mathcal{R}|1\rangle$ points along the instantaneous local magnetic field direction. In such a representation, the Hamiltonian is

$$H = \mathcal{R}^{-1}\frac{\mathbf{p}^2}{2m}\mathcal{R} + UJ_z/\hbar + i\hbar\frac{d\mathcal{R}^{-1}}{dt}\mathcal{R} \tag{19}$$

where

$$U = \mu B_0 + m\omega_\perp^2 \cos^2(\omega t)(x^2+y^2)/2. \tag{20}$$

Here we assume $m\omega_\perp^2(x^2+y^2) \ll \mu B_0$, so that the harmonic approximation is valid. We also neglect the effect of gravity. This latter assumption is relevant as long as $g \ll l_\perp \omega_\perp^2$, where $l_\perp = \sqrt{\hbar/(m\omega_\perp)}$ is the harmonic oscillator length. This condition ensures that the time-averaged potential is barely affected by the gravity and that the acceleration of the atoms over the spatial extension of the trapped state has a negligible effect.

We choose the rotation $\mathcal{R}$ as a product of a rotation along x and a rotation along y. To first order in x and y, $\mathcal{R}$ is

$$\mathcal{R} = 1 + i\theta_x J_x/\hbar + i\theta_y J_y/\hbar, \tag{21}$$

where the angles of the rotations along x and y are $\theta_x = -b'x\cos(\omega t)/B_0$ and $\theta_y = b'y\cos(\omega t)/B_0$, respectively. Here $b' = \omega_\perp\sqrt{2mB_0/\mu}$ is the quadrupole gradient at maximum current. Calculation to first order in θ_x, θ_y gives

$$\mathcal{R}^{-1}\frac{\mathbf{p}^2}{2m}\mathcal{R} = \frac{\mathbf{p}^2}{2m} + V_k \tag{22}$$

where

$$V_k = \frac{\sqrt{2}\hbar b'\cos(\omega t)}{mB_0}(p_x - ip_y)|0\rangle\langle 1| + \text{H.c.} \tag{23}$$

and H.c. stands for Hermitian conjugate. Here, we ignore the state $|-1\rangle$, which is relevant for low enough coupling (see below). The term V_k, due to the fact that $\mathcal{R}$ depends on the position, is responsible for spin-flip losses in time-independent Ioffe magnetic traps [23]. Within the approximations made here, the position dependence of $\mathcal{R}$ has no effect on the Hamiltonian within the spin state $|1\rangle$ manifold: the Coriolis coupling analyzed in [24], which corresponds to a rotation frequency proportional to b'^2, is not seen in this calculation.

Similar calculations give

$$i\hbar\frac{d\mathcal{R}^{-1}}{dt}\mathcal{R} = \frac{\hbar\omega b'}{\sqrt{2}B_0}\sin(\omega t)(x - iy)|0\rangle\langle 1| + \text{H.c.} \tag{24}$$

This term, due to the time modulation of the local spin orientation, may also produce spin-flip losses in modulated traps. The condition $\omega \gg \omega_\perp$ ensures that the term of Eq. (24) has an effect much larger than that of Eq. (23), and we neglect the latter in the following.

As in the previous section, we use the Floquet representation. The Hamiltonian H in the manifold of spin state $|1\rangle$ is decomposed into the term

$$H_0 = \sum_{n_F=-\infty}^{\infty} [p^2/2m + m\omega_\perp^2(x^2+y^2)/4 + n_F\hbar\omega]|1,n_F\rangle\langle 1,n_F| \tag{25}$$

and the term

$$H_2 = m\omega_\perp^2(x^2+y^2)/4\left(\sum_{n_F=-\infty}^{\infty}|1,n_F+2\rangle\langle 1,n_F| + \text{H.c.}\right) \tag{26}$$

that couples the Floquet n_F state to the Floquet states $n_F \pm 2$. Here, $|1,n_F\rangle$ is the state vector of an atom in the spin state $|1\rangle$ with the Floquet number n_F. The term H_2 is due to the part of Eq. (19) that is proportional to $\cos(2\omega t)$. Since we assumed $\omega \gg \omega_\perp$, the effect of H_2 is weak and can be treated perturbatively.

We will compute the loss rate of an atom initially in the spin state $|1\rangle$ of Floquet number $n_F=0$ and in the ground state ϕ_0 of H_0. The term of Eq. (24) couples this trapped state to the untrapped spin states $|0\rangle$ of Floquet numbers $n_F = \pm 1$. The energy spectrum of the spin state $|0\rangle$, which is unaffected by the magnetic field, is a continuum. Coupling to this continuum leads to a departure rate from the initial state, provided the Markov approximation is satisfied [25]. This approximation also ensures that the state $|-1\rangle$ can be neglected. We will show below that losses to the Floquet manifold $n_F=+1$ are much larger than losses to the Floquet manifold $n_F=-1$. Thus, we consider in the following the final states in the manifold $n_F=+1$. Since $i\hbar(d\mathcal{R}^{-1}/dt)\mathcal{R}$ does not affect the longitudinal motion, we concentrate on the transverse degrees of freedom and normalize ϕ_0 as $\iint dx\,dy|\phi_0|^2 = 1$. In addition, because $i\hbar(d\mathcal{R}^{-1}/dt)\mathcal{R}\phi_0$ is, up to a phase factor $e^{i\theta}$, invariant under a rotation of angle θ in the xy plane, the losses to spin 0 states are isotropic in the xy plane. It is thus sufficient to compute the departure rate toward a plane wave traveling in the x direction. The final state wave vector is

$$k_f = \sqrt{2m(\mu B_0 + \hbar\omega_\perp/\sqrt{2} - \hbar\omega)}/\hbar, \tag{27}$$

and the Fermi golden rule gives the departure rate

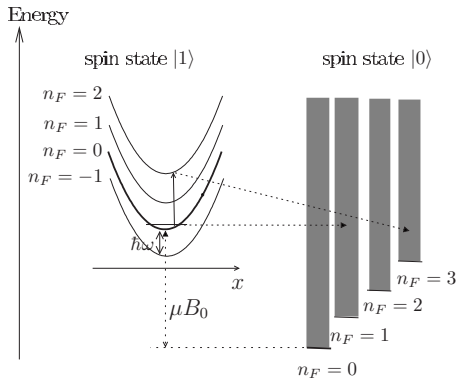

FIG. 5. Transitions responsible for spin-flip losses. For the spin state $|1\rangle$, the potential energy term of Eq. (25) is represented as well as the energy of the ground state in the $n_F=0$ manifold. For the spin state $|0\rangle$, we represented, for each Floquet manifold n_F, the whole energy spectrum, which is a semicontinuum starting at an energy $n_F\hbar\omega$. The transitions induced by the term of Eq. (24) are shown as dotted arrows, whereas transitions due to the term H_2 of Eq. (26) are shown as solid lines. The initial state is the spin state $|1\rangle$ of Floquet number $n_F=0$. For the two final Floquet states $n_F=1$ and 3, only the dominant processes are sketched, whose amplitudes are U_0 and U_1, respectively, where U_n is given in Eq. (29). In this picture, the odd Floquet state of $|0\rangle$ that is closest to resonance corresponds to $n_F=3$, and losses are dominated by Γ_1, where Γ_n is given in Eq. (30).

$$\Gamma_0 = \sqrt{2}\pi\frac{\omega^2}{m\mu B_0\omega_\perp}\hbar k_f^2 e^{-\sqrt{2}\hbar k_f^2/(m\omega_\perp)}. \tag{28}$$

The departure rate decreases exponentially with increasing bias field B_0, as for a usual time-independent Ioffe trap [23]. However, in the modulated trap, an additional exponential factor in $\omega/\omega_\perp$ reflects the fact that the Floquet level is increased by 1 while the spin is flipped. This transition is associated with the "emission" of a quantum of energy $\hbar\omega$, given to the oscillating magnetic field. Equation (28) also shows that the departure rate goes to zero for a modulation frequency very close to the frequency $\mu B_0/\hbar+\omega_\perp/\sqrt{2}$, i.e., for vanishing k_f. This cancellation is due to the fact that the coupling term of Eq. (24) is odd in x whereas the initial state is even and the final state, whose wave vector is vanishing, is flat. The departure rate toward the Floquet state $n_F=-1$ is identical to Eq. (28), ω being replaced by $-\omega$. Since we assumed $\omega\gg\omega_\perp$, the loss rate toward the Floquet state $n_F=-1$ is negligible compared to Eq. (28).

The condition $\omega\gg\omega_\perp$ and Eq. (28) show that the loss rate is exponentially small when ω reaches $\omega_1=(\mu B_0/\hbar+\omega_\perp/\sqrt{2})/3$, the value for which the initial state has the same energy as the untrapped state of Floquet number $n_F=3$ and of vanishing momentum. For modulation frequencies smaller than ω_1, second-order processes resonantly couple the initial state to the untrapped state $|0\rangle$ of Floquet number $n_F=3$. In these processes, represented in Fig. 5, the term H_2 of Eq. (26) first transfers the atoms into the virtually populated intermediate trapped state $|1\rangle$ of Floquet number $n_F=2$ before the term $i\hbar(d\mathcal{R}^{-1}/dt)\mathcal{R}$ realizes the transfer to the untrapped state $|0\rangle$ of Floquet number $n_F=3$. Although H_2 is weak, the loss rate associated with the second-order processes is much larger than the exponentially small Γ_0.

More generally, for a given modulation frequency, losses are dominated by transitions toward untrapped states of Floquet number $n_F=2n+1$ where $n=E((\mu B_0/\hbar+\omega_\perp/\sqrt{2})/(2\omega)-1/2)$, the function $E(x)$ being the integer part of x. Those transitions correspond to processes where the atom is first brought to the intermediate state $|1\rangle$ of Floquet number $n_F=2n$ by n transitions produced by the term H_2 and is then transferred to the untrapped state $|0\rangle$ of Floquet number $n_F=2n+1$ by the term $i\hbar\, d\mathcal{R}^{-1}/dt\,\mathcal{R}$ of Eq. (24). Perturbation theory gives an effective coupling between the state $|1\rangle$ of Floquet number $n_F=0$ and the states $|0\rangle$ of Floquet number $n_F=2n+1$ which is

$$U_n = -i\frac{\hbar\omega b'(x-iy)}{n!\,2\sqrt{2}B_0}[m\omega_\perp^2(x^2+y^2)/(16\hbar\omega)]^n. \tag{29}$$

The eigenstates of H_0 in the virtual intermediate states do not appear because, since we assumed $\omega\gg\omega_\perp$, the energy difference between the intermediate states is negligible and a resummation is possible.

The departure rate from the initial state toward the Floquet state $n_F=2n+1$ is computed from U_n using the Fermi golden rule. As for the calculation of Γ_0, it is sufficient to compute the departure rate in the x direction, and we obtain

$$\Gamma_n = \frac{m\omega^2 b'^2}{8\hbar B_0^2}\frac{(m\omega_\perp^2)^{2n}}{n!^2(16\hbar\omega)^{2n}}\left|\iint dx\,dy(x-iy)e^{ik_f x}\phi_0(x,y)\times(x^2+y^2)^n\right|^2, \tag{30}$$

where $k_f=\sqrt{2m[\mu B_0+\hbar\omega_\perp/\sqrt{2}-(2n+1)\hbar\omega]}/\hbar$ is the wave vector of the final state. Using the Gaussian expression for the ground state $\phi_0(x,y)$ in Eq. (30), we can show that Γ_n is the product of a polynomial in k_f and of the exponential factor $e^{-\sqrt{2}\hbar k_f^2/(m\omega_\perp)}$. The minima of the polynomial correspond to destructive interferences between the probability amplitudes of paths having different intermediate vibrational states. Since $\hbar k_f^2/m$ is reduced by 4ω when n is increased by 1 and since we assumed $\omega\gg\omega_\perp$, the exponential factor ensures, as stated above, that the total loss rate is dominated by the departure toward the highest Floquet subspace.

Figure 6 gives the departure rate of the trapped ground state as a function of ω for $\mu B_0=50\hbar\omega_\perp$. We observe several peaks that reflect the resonance behavior at integer values of $(\mu B_0+\omega_\perp/\sqrt{2}-\omega)/(2\omega)$. The height of the resonances goes down with increasing integer n as expected since the order of the transition increases with n. We verify that the loss rate is dominated by the losses toward the Floquet state of highest odd Floquet number, as expected. Between two resonances, we observe the expected exponential decrease of the loss rate. We observe a structure in the loss rate for losses to Floquet state larger than 1, as expected.

The lifetime of a thermal Maxwell-Boltzmann distribution is obtained after averaging the loss rate over the thermal distribution. In this calculation, ϕ_0 in Eq. (30) is replaced by the eigenstate $\phi_i(x)\phi_j(y)$, where i and j denote the vibra-

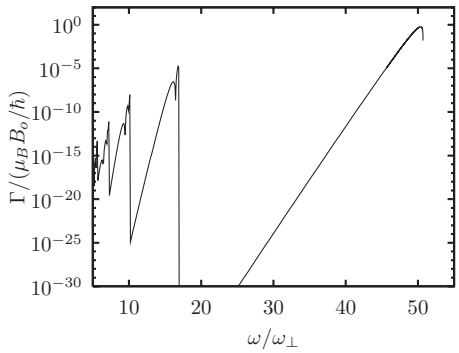

FIG. 6. Loss rate from the vibrational ground state versus the modulation frequency. The longitudinal magnetic field and the quadrupole gradient are chosen so that $\mu B_0/(\hbar\omega_\perp)=50$.

tional level. Neglecting changes of the final energy $\hbar^2k_f^2/(2m)$ across the thermal distribution, we can compute the departure rate Γ_0 for a Maxwell-Boltzmann distribution. More precisely, writing Eq. (30) as a fourth integral and using properties of Wigner functions we find, for temperatures $k_BT \gg \hbar\omega_\perp$,

$$\Gamma_0 = \frac{\pi^3}{2}\omega_\perp \frac{\hbar^3\omega_\perp\omega^2}{(k_BT)^3} e^{-(\mu B_0-\hbar\omega)/(k_BT)}. \tag{31}$$

Because of the crude approximation that the final energy does not depend on the initial state, this result is valid only up to a factor of the order of unity.

Experimentally, spin-flip losses can easily be avoided by properly choosing the modulation frequency. For example, let us assume that the transverse oscillation frequency of the instantaneous trap at maximum current is $\omega_\perp/(2\pi)=50$ kHz and the longitudinal magnetic field satisfies $B_0=50\hbar\omega_\perp/\mu$. If $\mu=\mu_B$ where μ_B is the Bohr magneton, this corresponds to $B_0=1.8$ G and the Larmor frequency $\mu B_0/\hbar$ is 2.5 MHz. In these conditions, the loss rate is dominated by the term Γ_0 of Eq. (28) as long as the modulation frequency is larger than 0.84 MHz and, in this frequency range, it is smaller than 1 s^{-1} as soon as $\omega<2.2$ MHz. For $\omega<0.84$ MHz, losses become dominated by transitions toward states of higher Floquet numbers, and the loss rate is peaked at modulation frequencies close to integer values of $\mu B_0/(2\hbar\omega)+\omega_\perp/(2\sqrt{2}\omega)-1/2$. In particular, the loss rate goes up to about 25 s^{-1} for a modulation frequency close to 0.8 MHz. Thus, the vicinity of this resonance should be avoided experimentally. Resonances of higher order are less problematic since the maximum loss rate they induce is smaller than 0.1 s^{-1}.

V. RADIO-FREQUENCY EVAPORATION IN THE MODULATED GUIDE

In this section we present general considerations on forced evaporation in a modulated guide. Since evaporative cooling is most efficiently realized in a three-dimensional (3D) trap, longitudinal confinement is required. A 3D trap can be obtained from the modulated guide of Sec. II by applying a z-dependent constant longitudinal field $B_0(z)$. Here, we consider evaporation in the transverse plane (xy) at a given z position and denote as B_0 the longitudinal magnetic field. For this purpose, in addition to the previous trapping potential, we apply a weak radio-frequency magnetic field polarized in the x direction, of frequency $\omega_{\rm rf}$ and of amplitude $B_{\rm rf}$. We consider here an atom of magnetic moment $\mu\mathbf{J}/\hbar$, where $\mathbf{J}$ is the atomic spin angular momentum.

Let us first give simple predictions, which rely only on the fact that, because of the modulation at 2ω of the trapping potential, the atomic Larmor frequency is modulated in time. The modulation amplitude $\delta\Omega$ increases, in the transverse plane, with the distance r from the trap center, according to $\delta\Omega=\mu b'^2r^2/(4\hbar B_0)$. Considering only the internal atomic dynamics at a given position, the modulation of the Larmor frequency is equivalent, within the rotating-wave approximation, to a frequency modulation of the radio-frequency field. In this picture, the radio-frequency spectrum consists of a carrier at the frequency $\omega_{\rm rf}$ and sidebands spaced by 2ω, the relative amplitude of the nth sideband with respect to the carrier being $J_n[\mu(b'r)^2/(8B_0\hbar\omega)]$, where J_n is the Bessel function of the first kind. Thus, for a given frequency of the applied rf field, the coupling to the untrapped state is resonant for the positions r_n such that

$$\omega_{\rm rf} = \mu B_0/\hbar + \mu b'^2 r_n^2/(4\hbar B_0) - 2n\omega, \tag{32}$$

where n is an integer. The coupling between the spin states close to a resonance position r_n is

$$V_n = V_0 J_n[\mu(b'r)^2/(8B_0\hbar\omega)] \tag{33}$$

where V_0 is the coupling produced by the radio-frequency field in the absence of modulation. Such a shell structure of the spin-flip transition resonances is characteristic of ac magnetic traps. For example, the same behavior is expected in TOP traps [26], where the Larmor frequency is also modulated in time.

In the following, we verify the statements made above by a more rigorous derivation. As in the previous section, we consider the representation in which the spin-up state points along the local instantaneous magnetic field. The rf field produces a term in the Hamiltonian experienced by the atoms which is, to first order in the angles $\theta_x=-b'x\cos(\omega t)/B_0$ and $\theta_y=b'y\cos(\omega t)/B_0$,

$$H_{\rm rf} = \mu B_{\rm rf}\cos(\omega_{\rm rf}t)J_x - \mu B_{\rm rf}b'y/B_0\cos(\omega_m t)\cos(\omega_{\rm rf}t)J_z. \tag{34}$$

The right-hand side is divided into two terms. The first term corresponds to the usual coupling between the spin states in the presence of the rf field. The second term appears due to the time dependence of $\mathcal{R}$. As in the previous section, in the following we consider the case of a spin-1 state and we restrict ourselves to the two spin states $|1\rangle$ and $|0\rangle$. We then have $H_{\rm rf_1}=H_{\rm rf_1}+H_{\rm rf_2}$, where

$$H_{\rm rf_1} = \mu B_{\rm rf}\cos(\omega_{\rm rf}t)(|1\rangle\langle 0| + |0\rangle\langle 1|)/\sqrt{2} \tag{35}$$

and

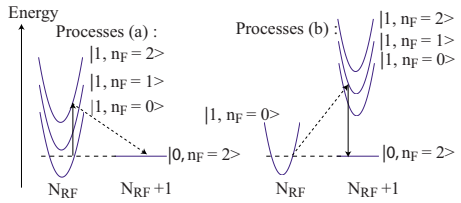

FIG. 7. (Color online) Processes involved in the transition from the trapped state $|1,n_F=0,N_{\rm rf}\rangle$ to the untrapped state $|0,n_F=2,N_{\rm rf}-1\rangle$. The process (a) involves the Hamiltonian H_2 of Eq. (26) (solid line) and the term $H_{{\rm rf}_1}$ of Eq. (35) (dashed line). The process (b) involves the term $H_{{\rm rf}_2}$ of Eq. (36) (dashed line) and the term $i\hbar\,\partial\mathcal{R}^{-1}/\partial t\,\mathcal{R}$ of Eq. (24) (solid line). For $\omega \ll \mu B_0$, the process (a) is dominant.

$$H_{{\rm rf}_2} = -\frac{\mu B_{\rm rf} b' y}{B_0}\cos(\omega_m t)\cos(\omega_{\rm rf} t)|1\rangle\langle 1|. \tag{36}$$

To analyze the effects of the rf field, we use the Floquet representation where two quantum numbers are used: the Floquet number n_F associated with the modulation frequency ω and $N_{\rm rf}$, the number of radio-frequency photons. We consider an atom in the trapped spin $|1\rangle$ state, with $N_{\rm rf}$ radio-frequency (rf) photons. Because $B_{\rm rf}$ is weak, we consider only transitions involving a single rf photon, and only those to the quasiresonant states where the spin is 0 and the number of rf photons is $(N_{\rm rf}+1)$.

Let us suppose the initial trapped state is in the $n_F=0$ manifold. The term $H_{{\rm rf}_1}$ couples the initial state to the spin 0 state in the manifold $|N_{\rm rf}+1,n_F=0\rangle$. This transition is resonant for the position r_0 given by Eq. (32) and the coupling to the spin-0 state is $\mu B_{\rm rf}/\sqrt{2}$. The initial state can also be transferred to the spin-0 state in the $|N_{\rm rf}+1,n_F=\pm 2\rangle$ manifolds by higher-order processes. These transitions, resonant for the position $r_{\pm 1}$ given by Eq. (32), can occur via two kinds of process, represented in Fig. 7 in the case where the final state lies in the manifold $n_F=2$. In the first process, H_2 of Eq. (26) couples the initial state to the spin-1 state in the manifold $|N_{\rm rf},n_F=\pm 2\rangle$, which is then transferred by the term $H_{{\rm rf}_1}$ to the spin-0 final state [process (a)]. In the second kind of process [process (b)], the transfer from the spin state 1 to the spin state 0 is ensured by the term $i\hbar(d\mathcal{R}^{-1}/dt)\mathcal{R}$ of the Hamiltonian [see Eq. (24)], and the term $H_{{\rm rf}_2}$ of the radio-frequency coupling is involved. In the case where $\omega \ll \mu B_0/\hbar$, the process (b) has a negligible amplitude and only the process (a) is important.

In a more general way, the initial state can be transferred to the final state of odd Floquet number $n_F=2n$, the transitions being resonant at the positions r_n given by Eq. (32). The dominant processes involve the first term $H_{\rm rf}$ given in Eq. (32) and the term H_2 to order n. The effective coupling between the trapped state and the spin-0 state of Floquet number $2n$, computed to lowest order in H_2, is

$$V_{n,\rm eff} = \frac{(-1)^n}{n!}\left(\frac{\mu b'^2 r^2}{16 B_0 \hbar\omega}\right)^{|n|}\frac{\mu B_{\rm rf}}{\sqrt{2}}. \tag{37}$$

We recover here the result of Eq. (33), in the limit considered here where $\hbar\omega \gg \mu b'^2 r^2/(8B_0)$. Thus the simple description in terms of frequency modulation of the Larmor frequency is sufficient to describe the physics.

In conclusion, we have shown that the radio-frequency field is resonant for different trap locations, whose potential energies differ by $2\hbar\omega/k_B$. For a modulation frequency of 50 kHz, the potential energy difference between two resonances is 3 μK. For a temperature of the order of 3 μK or higher, some resonances are present inside the atomic cloud and induce spin-flip losses. To overcome this problem, a precooling stage in a static trap down to temperatures smaller than 3 μK is required. For clouds whose temperature is smaller than 3 μK, the evaporation process in the modulated guide involves only one radio-frequency knife, so that the evaporative cooling is similar to that realized in a trap made by dc currents. Choosing the frequency of the radio-frequency field so that the transition involved in the cooling process is the transition that does not change the Floquet number is interesting for two reasons. First, as shown in Eq. (37), the coupling between the trapped and the untrapped state of this transition is larger than that of higher-order transitions that change the Floquet number. Second, this coupling is homogeneous and is thus constant when $\omega_{\rm rf}$ is chirped.

VI. CONCLUSION

The careful studies of the limitations of the modulation technique to smooth wire-guide roughness performed in this paper show that this technique is very robust and accepts a wide range of modulation frequencies. More precisely, on one side, we have shown that the unwanted effects of the modulation on the longitudinal motion are negligible for realistic parameters as long as modulation frequency is larger than 10 kHz: both the heating of the cloud and the remaining effective roughness are very small. On the other side, the calculation of the losses due to spin-flip transitions shows that, for realistic parameters, these losses are negligible as soon as the modulation frequency is smaller than a few hundreds of kilohertz. The modulation technique is thus a very promising tool that should enable atom-chip devices to be used to full advantage. In particular, the study of one-dimensional gases in the strongly interacting regime [27–29] on an atom chip can be considered.

The smoothing technique studied in this paper may be used in any situation where a rough potential is proportional to a quantity that can be modulated, so that the calculations developed in Sec. III may apply to other physical systems.

ACKNOWLEDGMENTS

The authors thank K. Mølmer for helpful discussions. The atom optics group of Laboratoire Charles Fabry is part of the IFRAF institute. This work was supported by the EU under Grants No. MRTN-CT-2003-505032 and No. IP-CT-015714.

APPENDIX A: DERIVATION OF THE ENERGY EXCHANGE RATE

The derivation of the heating rate follows that of the Fermi golden rule. For the calculation, we assume a quantification box of size L and periodic boundary conditions. We

assume the atom is initially in the state of momentum p_0 in the Floquet subspace $n_F=0$. For simplicity we consider only the transitions toward the Floquet state $n_F=-1$. After a time t much smaller than the departure rate, the change in kinetic energy ΔE can be deduced from perturbation theory, and we obtain

$$\Delta E = \sum_q |u_q|^2 f(q,t). \tag{A1}$$

Here $u_q=\int dz\, u(z)e^{iqz}/L$ is the Fourier component of wave vector q of $u(z)$ and

$$f(q,t) = (\epsilon - \hbar\omega)\frac{\sin^2(\epsilon t/2)}{\epsilon^2}, \tag{A2}$$

where $\epsilon=\hbar\omega+\hbar^2q^2/(2m)+\hbar p_0 q/m$ is the energy change associated with the transition involving the Fourier component of u of wave vector q. The terms u_q are uncorrelated complex random numbers of mean square value $\langle|u_q|^2\rangle = S(q)L/(2\pi)$, where $S(q)=(1/2\pi)\int dz\, e^{iqz}\langle u(z)u(0)\rangle$ is the spectral density of u. For a large enough quantification box, the term $f(q)$ barely changes between adjacent Fourier components and one can replace $\Sigma_q|u_q|^2 f(q)$ by $\int dq\, S(q)f(q)$ in Eq. (A1). For a time t large enough so that the function $(\epsilon-\hbar\omega)S(q(\epsilon))$ is about constant on the interval $\epsilon\in[-\hbar/t,\hbar/t]$, the term $\sin^2(\epsilon t/2)/\epsilon^2$ can be replaced by the distribution $t\delta(\epsilon)\pi/2$. We then recover the first term of Eq. (4). The previous condition on t and the condition that t is much smaller than the departure rate Γ can be satisfied simultaneously only if the function $(\epsilon-\hbar\omega)S(q(\epsilon))$ is about constant on the interval $\epsilon\in[-\hbar\Gamma,\hbar\Gamma]$. This is the condition of the Markovian approximation. This condition is satisfied provided that both $S(q)$ and its correlation length are small enough.

The calculation is similar for losses toward the Floquet manifold $n_F=1$, and one finally recovers Eq. (4). The Markovian condition for the transition toward the Floquet manifold $n_F=1$ is not satisfied for initial momentum very close to $\sqrt{2m\hbar\omega}$ since the atoms are then sensitive to the fact that the continuum is not infinite for $\epsilon<0$. Similar non-Markovian situations have been studied, for example, in photonic band gap materials [30], and oscillatory behavior and decay toward a nonvanishing population of the initial state are expected.

APPENDIX B: ADIABATIC POTENTIAL IN THE DRESSED STATE REPRESENTATION

In this appendix, we rederive the adiabatic potential given in Eq. (14) using a dressed representation, where a local z-dependent unitary transformation $\mathcal{O}(z)$ is applied to the Floquet states so that the resulting dressed states $|n\rangle(z)$ are eigenstates of the potential energy part of the Floquet Hamiltonian [the term $\hbar\omega n_F$ of H_0 given in Eq. (2) and the term H_2 of Eq. (3)]. By symmetry, the energy of the dressed states $|n\rangle(z)$ is $n\hbar\omega$, like that of the bare Floquet states. Using the properties of the Bessel functions $[J_{k+1}(x)+J_{k-1}(x)]x/(2k)=J_k(x)$ and $\Sigma_n J_n(x)^2=1$, we show that the decomposition of $|n\rangle(z)$ in the undressed Floquet basis ($|k\rangle_0$) is

$$|n\rangle(z) = \sum_{k=-\infty}^{\infty} J_k[u(z)/\omega]|n+k\rangle_0 = \mathcal{O}(z)|n\rangle_0. \tag{B1}$$

This well-known result has been used in several other situations [31]. In the dressed state representation, the state of the system is $\tilde{\psi}=\mathcal{O}^{-1}\psi_0$, where ψ_0 is the state of the system in the undressed representation and the momentum operator, $\tilde{p}=\mathcal{O}^{-1}p\mathcal{O}$, is

$$\tilde{p} = p - \sum_{n,k} \langle k,z|i\hbar\partial_z|n,z\rangle|k\rangle\langle n| \tag{B2}$$

where $p=-i\hbar\partial_z$ is the momentum operator that preserves the Floquet number and ∂_z is a shorthand notation for ∂/∂_z. Thus, in the dressed state representation, the Hamiltonian is decomposed into three terms:

$$\tilde{H}_0 = p^2/2m - n_F\hbar\omega, \tag{B3}$$

which does not couple different Floquet states,

$$\tilde{H}_1 = -(\hbar/2m)\Big(p\sum\nolimits_{n_1,n_2}|n_1\rangle\langle n_1|i\partial_z|n_2\rangle\langle n_2| + \sum\nolimits_{n_1,n_2}|n_1\rangle\langle n_1|i\partial_z|n_2\rangle\langle n_2|p\Big), \tag{B4}$$

and

$$\tilde{H}_2 = -(\hbar^2/2m)\sum_{n_1,n_2,n_3}|n_1\rangle\langle n_2|\langle n_1|\partial_z|n_3\rangle\langle n_3|\partial_z|n_2\rangle. \tag{B5}$$

Since $J_k'=(J_{k-1}-J_{k+1})/2$ and $\Sigma_k J_k J_{k+n}=\delta_n$, $\tilde{H}_1$ couples adjacent Floquet states. This term is responsible for the heating of the cloud. On the other hand, $\tilde{H}_2$ contains a term $\tilde{H}_{2,\mathrm{ad}}$ that does not change the Floquet number. Using the above properties of the Bessel function, we find that $\tilde{H}_{2,\mathrm{ad}}$ is just the adiabatic potential of Eq. (14).

[1] R. Folman, P. Krüger, J. Schmiedmayer, J. Denschlag, and C. Henkel, Adv. At., Mol., Opt. Phys. **48**, 263 (2002), and references therein.

[2] Y.-J. Wang, D. Z. Anderson, V. M. Bright, E. A. Cornell, Q. Diot, T. Kishimoto, M. Prentiss, R. A. Saravanan, S. R. Segal, and S. Wu, Phys. Rev. Lett. **94**, 090405 (2005).

[3] T. Schumm, S. Hofferberth, L. M. Andersson, S. Wildermuth, S. Groth, I. Bar-Joseph, J. Schmiedmayer, and P. Krüger, Nat. Phys. **1**, 57 (2005).

[4] A. Gunther, S. Kraft, C. Zimmermann, and J. Fortagh, Phys. Rev. Lett. **98**, 140403 (2007).

[5] J. Esteve, J.-B. Trebbia, T. Schumm, A. Aspect, C. I. Westbrook, and I. Bouchoule, Phys. Rev. Lett. **96**, 130403 (2006).

[6] J.-B. Trebbia, J. Esteve, C. I. Westbrook, and I. Bouchoule,

Phys. Rev. Lett. **97**, 250403 (2006).
[7] J. Reichel and J. H. Thywissen, J. Phys. IV **116**, 265 (2004).
[8] D. W. Wang, M. D. Lukin, and E. Demler, Phys. Rev. Lett. **92**, 076802 (2004).
[9] J. Estève, C. Aussibal, T. Schumm, C. Figl, D. Mailly, I. Bouchoule, C. I. Westbrook, and A. Aspect, Phys. Rev. A **70**, 043629 (2004).
[10] J.-B. Trebbia, C. L. Garrido Alzar, R. Cornelussen, C. I. Westbrook, and I. Bouchoule, Phys. Rev. Lett. **98**, 263201 (2007).
[11] W. Petrich, M. H. Anderson, J. R. Ensher, and E. A. Cornell, Phys. Rev. Lett. **74**, 3352 (1995).
[12] S. Kraft, A. Günther, H. Ott, D. Wharam, C. Zimmermann, and J. Fortàgh, J. Phys. B **35**, L469 (2002).
[13] These two requirements are also needed for the TOP trap to work.
[14] T. Schumm, J. Esteve, C. Figl, J. Trebbia, C. Aussibal, D. Mailly, I. Bouchoule, C. Westbrook, and A. Aspect, Eur. Phys. J. D **32**, 171 (2005).
[15] R. J. Cook, D. G. Shankland, and A. L. Wells, Phys. Rev. A **31**, 564 (1985).
[16] J. H. Shirley, Phys. Rev. **138**, B979 (1965).
[17] E. Landau and E. Lifschitz, *Mechanics* (Mir, Moscow, 1980), Chap. 5.
[18] R. F. Wuerker, H. Shelton, and R. V. Langmir, J. Appl. Phys. **30**, 342 (1959).
[19] D. Leibfried *et al.*, Rev. Mod. Phys. **75**, 281 (2003).
[20] R. Geursen, N. R. Thomas, and A. C. Wilson, Phys. Rev. A **68**, 043611 (2003).
[21] J. H. Müller, O. Morsch, D. Ciampinin, M. Anderlini, R. Mannella, and E. Arimondo, Phys. Rev. Lett. **85**, 4454 (2000).
[22] E. Brion, L. H. Pedersen, and K. Mølmer, e-print arXiv:quant-ph/0610056.
[23] C. V. Sukumar and D. M. Brink, Phys. Rev. A **56**, 2451 (1997).
[24] T.-L. Ho and V. B. Shenoy, Phys. Rev. Lett. **77**, 2595 (1996).
[25] G. M. Moy, J. J. Hope, and C. M. Savage, Phys. Rev. A **59**, 667 (1999).
[26] J. L. Martin *et al.*, J. Phys. B **33**, 3919 (2000).
[27] B. Laburthe Tolra, K. M. O'Hara, J. H. Huckans, W. D. Phillips, S. L. Rolston, and J. V. Porto, Phys. Rev. Lett. **92**, 190401 (2004).
[28] B. Paredes *et al.*, Nature (London) **429**, 277 (2004).
[29] T. Kinoshita, T. Wenger, and D. S. Weiss, Science **305**, 1125 (2004).
[30] S. John and T. Quang, Phys. Rev. A **50**, 1764 (1994).
[31] A. Eckardt, T. Jinasundera, C. Weiss, and M. Holthaus, Phys. Rev. Lett. **95**, 200401 (2005); S. Haroche *et al.*, *ibid.* **24**, 861 (1970).